Nanoscale

Accepted Manuscript

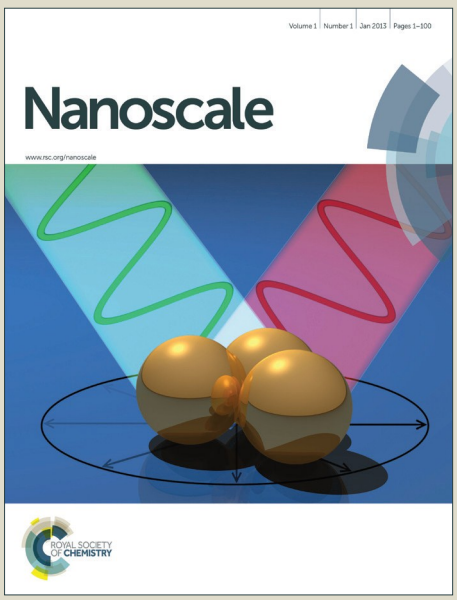

ROYAL SOCIETY OF CHEMISTRY

www.rsc.org/nanoscale

Journal Name

COMMUNICATION

Evaluation of Blood-Brain Barrier-Stealth Nanocomposites for *in situ* Glioblastoma Theranostic Applications

Received 00th January 20xx,
Accepted 00th January 20xx

DOI: 10.1039/x0xx00000x

www.rsc.org/

Chia-Hao Su,[a,b,‡] Ching-Yi Tsai,[a,‡] Boguslaw Tomanek,[c] Wei-Yu Chen [a] and Fong-Yu Cheng*[d]

The blood-brain barrier (BBB) is a physiological structure of the blood vessels in the brain. The BBB efficiently traps most therapeutic drugs in the blood vessels and stops them from entering the brain tissue, resulting in decreased therapeutic efficiency. In this study, we developed BBB-stealth nanocomposites composed of iron oxide (Fe_3O_4) nanoparticles (NPs) as a safe nanocarrier for glioblastoma therapy. We showed antitumor activity of Dox/alg-Fe_3O_4 NPs using *in vitro* and *in vivo* tests. We demonstrated G23-alg-Fe_3O_4 NPs crossed the BBB and entered the brain. *In situ* glioblastoma tumor-bearing mice were established to successfully evaluate the antitumor activity of G23-Dox/alg-Fe_3O_4 NPs. Magnetic resonance imaging (MRI) and bioluminescence imaging (BLI) confirmed BBB crossing. The BBB-stealth nanocomposites show large potential for a proof-of-concept clinical trial as a theranostic platform for human brain tumor therapy.

Glioblastoma is the most aggressive type of brain tumor, with an extremely low percentage of survivors.[1] Many drugs can effectively kill glioma cells *in vitro,* but they cannot inhibit them *in vivo* because of their poor solubility and short circulation time. These critical obstacles can be overcome by using drug/nanoparticle (NP) complexes. The advantages of drug/NP complexes include prolonged circulation time and enhanced drug delivery.[2] However, the blood-brain barrier (BBB) is a major interface between the blood and the brain and limits the brain's uptake of therapeutic agents, which results in reduced therapeutic efficiency.[3,4] Hence, developing effective platforms that can deliver drugs across the BBB is extensive and urgent.

NPs had been proved to effectively increase drug delivery to the brain.[5] Safety of NPs is a critical concern due to importance of the brain for humans and animals. Ideally, NPs must be biocompatible, biodegradable, and non cytotoxic. Therefore application of U.S. Food and Drug Administration (FDA)-approved materials is prefered for clinical trials. Thus, application of most NPs, except gold (Au), iron oxide, and liposome NPs for brain diseases is largely limited. Au and liposome NPs are used to treat brain diseases due to their excellent biocompatibility and low cytotoxicity.[6] However, Au and liposome NPs lack the detection ability in MRI, a powerful modality for detecting brain and other diseases, unless they are conjugated with gadolinium (Gd^{3+}) ions[7] or iron oxide NPs.[8] The synthesis processes of functionalization of gold or liposome NPs for MR applications are complex and cumbersome. Application of magnetic nanomaterials as primary nanocarriers can directly enable their MRI usage. Herein, we report the development of an anticancer drug (doxorubicin [Dox]) nanocarrier composed of Fe_3O_4 NPs and alginate tagged with BBB-permeating G23 peptides (sequence: HLNILSTLWKYRC) on the particle surface. This nanocarrier is able to cross the BBB and enter the brain to treat glioblastoma, both *in vitro* and *in vivo* (Scheme 1). Importantly, Fe_3O_4 and alginate are authorized for human use by the U.S. FDA and their metabolites are safe in human bodies with no side effects in applied doses.

The alginate-conjugated Fe_3O_4 NPs (alg-Fe_3O_4 NPs) were prepared by using carbodiimide reaction to conjugate alginate on the NH_2-exposed Fe_3O_4 NPs (NH_2-Fe_3O_4 NPs) as previously described.[9] Transmission electron microscopy (TEM) images show that the real diameters (RDs) of NH_2-Fe_3O_4 NPs and alg-Fe_3O_4 NPs are respectively 6.5 nm and 6.8 nm (Fig. S1a). The hydrodynamic diameters (HDs) of NH_2-Fe_3O_4 NPs and alg-Fe_3O_4 NPs are 13.6 nm and 120.4 nm respectively as measured by dynamic light scattering. The large HD of the alg-Fe_3O_4 NPs is due to the presence of alginate on the particle surface. The surface charge of the NH_2-Fe_3O_4 NPs was +20.1 mV. After conjugation with alginate, the surface charge of the alg-Fe_3O_4 NPs was –44.6 mV. This change indicates the alginate was tagged on the NH_2-Fe_3O_4 NPs. Fourier transform infrared spectroscopy (FT-IR) was also used to confirm alginate on the Fe_3O_4 NP surface (Fig. S1b). Both characteristic peaks of Fe_3O_4

[a] *Institute for Translational Research in Biomedicine, Kaohsiung Chang Gung Memorial Hospital, Kaohsiung 833, Taiwan.*
[b] *Department of Biomedical Imaging and Radiological Sciences, National Yang Ming University, Taipei 112, Taiwan.*
[c] *Institute of Nuclear Physics, Polish Academy of Sciences, 152 Radzikowskiego, Krakow, Malopolska, 31-342, Poland.*
[d] *Institute of Oral Medicine, National Cheng Kung University Hospital , College of Medicine, National Cheng Kung University, 1 University Road, Tainan City 701, Taiwan. E-mail: FYCheng@mail.ncku.edu.tw*
‡ *These authors contributed equally to this study.*
† Electronic Supplementary Information (ESI) available: [Experimental details]. See DOI: 10.1039/x0xx00000x

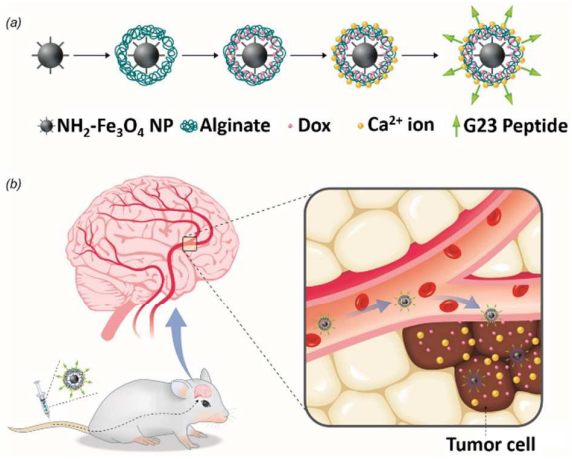

Scheme 1 a) Schematic synthesis process of BBB-stealth nanocarriers. b) Schematic mechanism of BBB-stealth nanocarriers and then Dox release from nanocarriers to brain tissue to kill tumor cells.

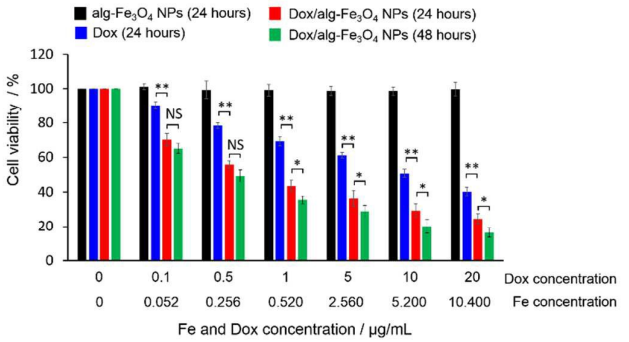

Fig. 1 *In vitro* cell viability of C6 cells incubated with free Dox, alg-Fe_3O_4 NP, and Dox/alg-Fe_3O_4 NPs at 37°C for 24 and 48 h. All experiments were repeated in triplicate. (*, $p < 0.05$; ***, $p < 0.001$; NS, not significant)

NPs and alginate were appeared in FT-IR spectrum of the alg-Fe_3O_4 NPs.

To fabricate the Dox-encapsulated alg-Fe_3O_4 NPs (Dox/alg-Fe_3O_4 NPs), the surface alginate of NPs was crosslinked by Ca^{2+}, and then Dox was trapped inside the NPs. The RD and HD of Dox/alg-Fe_3O_4 NP were 6.9 nm and 124.2 nm respectively. The surface charge of Dox/alg-Fe_3O_4 NP was -19.3 mV. TEM image of Dox/alg-Fe_3O_4 NPs (Fig. S1a) show no aggregation after crosslinking by Ca^{2+}. The saturated capacity of Dox in Dox/alg-Fe_3O_4 NPs was ~1.39 mg Dox per mg of Fe_3O_4 NPs (Fig. S2). To evaluate the Dox-trapped efficiencies of Dox/alg-Fe_3O_4 NPs, the Dox leaching of Dox/alg-Fe_3O_4 NPs that had been crosslinked by different Ca^{2+} concentrations were tested in deionized water and phosphate buffered saline (PBS) (10 mM, pH 7.4) at 37°C (Fig. S3). The maximum leaching percentage (~18%) of Dox was observed in 0.1 mM Ca^{2+}-treated Dox/alg-Fe_3O_4 NPs in PBS after 96 h. Except for the above condition, the leaching percentages of Dox in other conditions in Fig. S3 are below 10% after 240 h. These results indicate that using concentrations of Ca^{2+} > 1 mM to crosslink alginate efficiently trapped Dox in the Dox/alg-Fe_3O_4 NPs. The Dox leaching percentage in PBS is higher than in deionized water because some constituents of PBS, such as sodium (Na^+) and potassium ions (K^+), can destroy the crosslink of Ca^{2+} and alginate. Fig. S4 shows the Dox release profiles of different Ca^{2+} concentration-treated Dox/alg-Fe_3O_4 NPs in PBS (pH 5.5) and cytoplasm mimicking (CM) buffer at 37°C. All Dox-release percentages of 0.1, 1, and 10 mM Ca^{2+}-treated Dox/alg-Fe_3O_4 NPs were faster and higher in CM buffer than in PBS (pH 5.5). The Dox-release rate of Dox/alg-Fe_3O_4 NPs in CM buffer was faster than in PBS (pH 5.5) because of the ethylene-bis(oxyethylenenitrilo) tetraacetic acid (EGTA) in the CM buffer. EGTA can strongly grab the Ca^{2+} chelated with the alginate of the Dox/alg-Fe_3O_4 NPs and destroy the crosslink structures. Compared with CM buffer, the Dox release rate in PBS (pH 5.5) was slower because PBS (pH 5.5) provided only protons to transfer some COO^- groups of alginate to COOH groups, except for the Na^+ and K^+ constituents. However, PBS (pH 7.4) can interfere only with the alg-Na^+ and alg-K^+ crosslinks; thus, the Dox release rates in Fig. S3 are very low. Based on the results of Dox leaching and release tests of Dox/alg-Fe_3O_4 NPs (Fig. S3 and S4), Dox/alg-Fe_3O_4 NPs treated with higher concentrations of Ca^{2+} provided a higher degree of crosslinking with alginate and either inhibited or decreased the amount of Dox released at the same time. Therefore, 1 mM Ca^{2+}-treated Dox/alg-Fe_3O_4 NPs were better and selected for further *in vitro* and *in vivo* tests.

To determine safe doses of Dox/alg-Fe_3O_4 NPs for cell and animal experiments, an MTT assay was used to evaluate cell viability. Human umbilical vein endothelial cells (HUVECs) were incubated with different Fe doses of alg-Fe_3O_4 NPs at 37°C for 24 and 48 h. The alg-Fe_3O_4 NPs showed no obvious cytotoxicity and the HUVECs had viability rates > 95% (Fig. S5). Subsequently, an MTT assay showed that cell viability of C6 brain cancer cells (rat glioma) was > 95% after 24 h of incubation with alg-Fe_3O_4 NPs at 37°C (Fig. 1). To evaluate efficacy of the Dox/alg-Fe_3O_4 NPs, C6 cells were separately treated with Dox and Dox/alg-Fe_3O_4 NPs for 24 h. Cell viability was significantly lower in Dox/alg-Fe_3O_4 NP-treated C6 cells than in free-Dox-treated C6 cells because the NPs increased the amount of drugs delivered to the cells.[10] After 48 h of treatment with the Dox/alg-Fe_3O_4 NPs, C6 cell viability was further decreased.

To investigate the BBB-stealth function of the alg-Fe_3O_4 NPs, the G23 peptide-conjugated alg-Fe_3O_4 NPs (G23-alg-Fe_3O_4 NPs) were prepared and a mouse cerebral endothelial cell line (bEnd3) was used to demonstrate the NP transport across the BBB.[11] The RD and HD of G23-alg-Fe_3O_4 NP were 7.0 nm and 137.5 nm respectively and its surface charge was -14.2 mV. G23 peptide can promote transport of NPs across the BBB by targeting gangliosides.[12] The G23-alg-Fe_3O_4 NPs and the alg-Fe_3O_4 NPs did not damage the bEnd3 cells (Fig. 2a). Thus, the notion that the cell disruption allows NPs to cross the BBB can be excluded. The *in vitro* BBB-stealth efficacy of the G23-alg-Fe_3O_4 NPs was measured using transwell filters.[11,13] Fig. 2b shows a schematic overview of a transwell assay for the G23-alg-Fe_3O_4 and alg-Fe_3O_4 NPs. The content of the Fe_3O_4 NPs on the apical (AP) and basolateral (BL) using inductively coupled plasma optical emission spectrometry. The G23-alg-Fe_3O_4 NPs apparently have BBB-stealth efficiency of ~35.4%, but the alg-Fe_3O_4 NPs have low efficiency of only ~5.3% (Fig. 2c). The G23 peptide appears to account for the obvious difference in BBB-

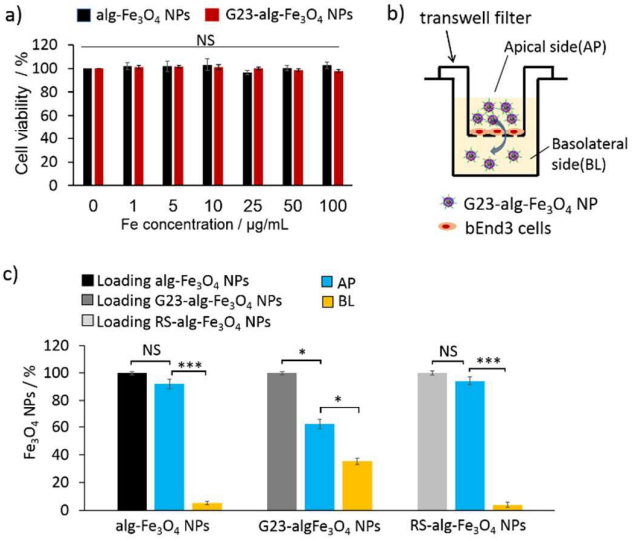

Fig. 2 a) *In vitro* cell viability of bEnd3 cells incubated with the alg-Fe_3O_4 NPs and G23-alg-Fe_3O_4 NPs with a series of Fe concentrations at 37°C for 24 h. b) Schematic overview of the *in vitro* bEnd3 cell transwell assay. c) The transcytosis percentages of the alg-Fe_3O_4 NPs and G23-alg-Fe_3O_4 NPs relative to the doses of the alg-Fe_3O_4 and G23-alg-Fe_3O_4 NPs loaded, respectively. The Fe doses of the alg-Fe_3O_4, G23-alg-Fe_3O_4, and RS-alg-Fe_3O_4 NPs were 10 μg/mL. All experiments were repeated in triplicate. (*, $p < 0.05$; ***, $p < 0.001$; NS, not significant)

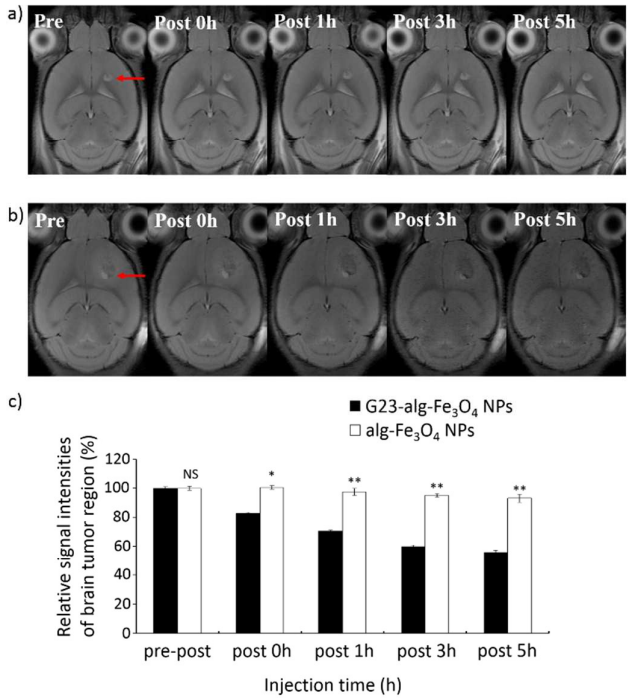

Fig. 3 *In vivo* MR imaging monitored and contrastt enhancement using a 9.4 T animal micro MRI system. MR coronal imaging of the brain tumor with intravenous injection of a) alg-Fe_3O_4 NPs and b) G23-alg-Fe_3O_4 NPs as a function of the exposure period, and c) the corresponding MR signal intensity (N=6). (*, $p < 0.05$; **, $p < 0.01$; NS, not significant)

stealth efficiency between the G23- alg-Fe_3O_4 and alg-Fe_3O_4 NPs. To further confrim the BBB-stealth efficiency of G23-alg-Fe_3O_4 NPs come from the function of G23 peptide, random sequence peptide (LTCNLHKYSRWL)-conjugated alg-Fe_3O_4 NP (RS-alg-Fe_3O_4 NPs) were prepared and evaluted their BBB-stealth efficacy (Fig. 2c). The RS-alg-Fe_3O_4 NPs have low efficiency of only ~4.1%. This indicate G23 peptide of G23-alg-Fe_3O_4 NP certainly play an important role in crossing the BBB by targeting ganglioside, not by a non-specific binding with the BBB.

In order to further confirm the safety and effect of G23-alg-Fe_3O_4 NPs for the BBB, the *in vivo* BBB integrity tests of mice were evaluted in this study. We used evans blue staining to evaluate and observe the BBB integrity assay in different animal conditions (shown in Fig. S6). As the result, we could not find any difference in brain tissues of sham control (PBS-treated mice), G23-alg-Fe_3O_4 NP-treated mice, and U87MG-luc2 tumor baring mice. Contrarily, we could find the evans blue staining in stroke model (positive control), it is indicated that the BBB was broken in the infarct area of stroke.

We demonstrated the contrast efficiency and potential of the G23-alg-Fe_3O_4 NPs for permeation across the BBB and for brain MRI *in vivo* using BALB/c mice. Firstly, the r1 and r2 relaxivities of the alg-Fe_3O_4 NPs were separately measured and calculated to be 5.4 and 43.8 $s^{-1}mM^{-1}$ in a 9.4 T field strength. For G23-alg-Fe_3O_4 NPs, the r1 and r2 relaxivities were 4.5 and 37.9 $s^{-1}mM^{-1}$ at the same condition. The mice were intravenously injected with the alg-Fe_3O_4 or G23-alg-Fe_3O_4 NPs, and coronal and axial T_2-weighted MRI was done with a 9.4 T animal MRI system pre-injection, immediately post-injection, and then 1 and 3 h post-injection. Mice injected with the G23-alg-Fe_3O_4 NPs showed stronger contrast-enhancement in T_2-weighted images than did mice injected with the alg-Fe_3O_4 NPs.

The brain nucleus MR images were contrast-enhanced (Fig. S7a) as were the caudate putamen (Cpu) (Fig. S7b) and olfactory bulb (OB) (Fig. S7c). Remarkably, when the G23-alg-Fe_3O_4 NPs crossed the BBB and entered the brain tissue, the fine structure was highlighted, especially in the OB and hippocampus. Moreover, the T2-weighted images of the brains of mice treated with the G23-alg-Fe_3O_4 NPs were contrast enhanced 24 h post-injection (Fig. S8a), and the signal intensities of the OB slightly recovered (Fig. S8b). To evaluate the efficiency of the T_2 contrast enhancement, the relative signal intensities of T_2-weighted images in the OB, Cpu, hippocampus, and brain stem were calculated (Fig. S9). Moreover, the MR contrast and BBB-stealth efficiency of the alg-Fe_3O_4 NPs was not significant at the same dose, nor was signal change in the brain nucleus (Fig. S10). Contrarily, 3 h post-injection the G23-alg-Fe_3O_4 NPs showed contrast effects in decreased signal intensities (down to 70% in the OB, 80% in the Cpu, 80% in the hippocampus, and 64% in brain stem) was observed. Compared with the *in vitro* BBB-permeating assay, G23-alg-Fe_3O_4 NPs permeated the BBB and showed excellent contrast enhancement for brain MRI.

To investigate the therapeutic effects of future clinical applications of the G23-Dox/alg-Fe_3O_4 NPs (RD: 7.0 nm; HD: 139.6 nm; surface charge: -12.2 mV) for *in vivo* and *in situ* human brain cancer, animal model of U87MG-luc2 (human glioblastoma cell line) tumor bearing mice was established. The application of the G23-alg-Fe_3O_4 NPs for MRI of brain tumor was evaluated 9 days after tumor cell injection. The alg-Fe_3O_4 and G23-alg-Fe_3O_4 NPs were administrated by

intravenous injection at a Fe dosage of 10 mg kg^{-1}. Efficacy of the NPs as a contrast agent, measured as signal changes was monitored with pre- and post-injection MRI. The alg-Fe_3O_4 NPs did not show any contrast enhancement in the brain tumor even 5 h post injection (Fig. 3a). Contrarily, the G23-alg-Fe_3O_4 NPs could penetrate the BBB and resulted in a signal decrease in tumor regions at different injection times (Fig. 3b). The quantitative analysis showed a contrast decrease over time. The tumor signal was reduced to 56% 5 h post injection of the G23-alg-Fe_3O_4 NPs (Fig. 3c). This indicates that the G23 peptide helps the NPs to cross the BBB and accumulates at the tumor site in larger quantities, as shown by significant negative contrast effect. Brain tumor tissue samples were also analyzed using Pearl's iron stain (Fig. S11). The tissue showed light bluish-purple staining in mice treated with the G23-alg-Fe_3O_4 NPs, but only pinkish background staining in the brains of the alg-Fe_3O_4 NP-treated mice. These results provided evidence that G23 peptides increase the BBB-stealth of NPs. To demonstrate the therapeutic functions of G23-alg-Fe_3O_4 NPs, free Dox, Dox/alg-Fe_3O_4 NPs, G23-alg-Fe_3O_4 NPs and G23-Dox/alg-Fe_3O_4 NPs were intravenously injected, and the tumor size and bioluminescence (BL) imaging were then monitored pre-injection and at 3 and 7 days post-injection using the IVIS image system (Fig. 4). The quantitative results of the BL images in each group were shown in Fig. S12. Tumors continuously grew in PBS-treated mice. In the mice treated with Dox, alg-Fe_3O_4 NPs and G23-alg-Fe_3O_4 NPs, the tumor sizes showed no obvious variation until 7 days post-injection. Tumors shrank significantly in the mice treated with G23-Dox/alg-Fe_3O_4 NPs. It seems that releasing the Dox directly inside the tumor cells yielded more efficacious anti-tumor activity by G23-Dox/alg-Fe_3O_4 NPs. By contrast, in the free Dox- and Dox/alg-Fe_3O_4 NP-treated mice, Dox and Dox/alg-Fe_3O_4 NPs remained outside the BBB and had no anti- tumor effect. In the G23-alg-Fe_3O_4 NP-treated mice, G23-alg-Fe_3O_4 NPs could cross the BBB, but they lacked Dox to kill tumor cells.

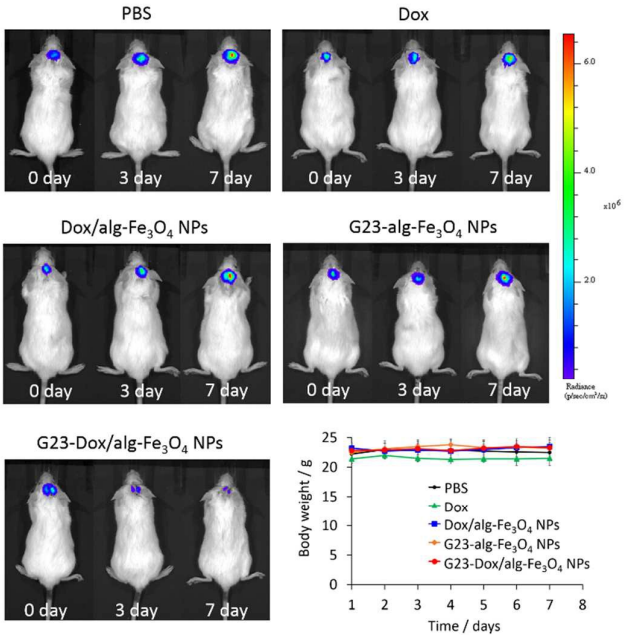

Fig. 4 *In vivo* anti-tumor activity of the Dox/alg-Fe_3O_4 NPs in mice with U87MG-luc2 tumors ~50 mm^3 during the experimental period. All images are luminescence images from U87MG-luc2 cells monitored using the IVIS imaging system. The mice (N= 5) were intravenously injected with PBS, Dox, Dox/alg-Fe_3O_4 NPs, G23-alg-Fe_3O_4 NPs, and G23-Dox/alg-Fe_3O_4 NPs. The injected Dox dose was 3 mg/kg of body weight and the equivalently injected Fe dosage was 10 mg/kg of body weight.

In summary, a novel BBB-stealth nanocomposite composed of U.S. FDA-approved Fe_3O_4 NPs and alginate has been synthesized. The NPs can encapsulate Dox and be conjugated with G23 peptides on their surface. Dox can be released from the G23-Dox/alg-Fe_3O_4 NPs after cellular uptake. Both *in vitro* and *in vivo* experimental results showed that the Dox/alg-Fe_3O_4 NPs efficiently inhibited C6 tumor cell growth or killed them. We also confirmed that the G23-alg-Fe_3O_4 NPs can cross the BBB and provide efficient anti-brain-tumor therapy in *in situ* U87MG-luc2 tumor-bearing mice. We anticipate that these BBB-stealth NPs will provide even more potential in future clinical trials and other brain disorders.

Acknowledgements

We thank the molecular imaging core of the Institute for Translational Research in Biomedicine, Kaohsiung Chang Gung support on IVIS Spectrum and 9.4T animal MRI. This work was supported by the Ministry of Science and Technology, Taiwan (MOST 101-2113-M-006-006, 104-2923-M-006-002, 103-2320-B-182A-004, and 103-2633-B-182A-001) and the National Centre for Research and Development, Poland, the Headquarters of University Memorial Hospital, Kaohsiung, Taiwan for technical and material Advancement at National Cheng Kung University, Tainan, which is sponsored by the Taiwan Ministry of Education, and grant CMRPG8C1171 and CMRPG8C1172 from Chang Gung Medical Foundation, Taiwan.

References

1 J. T. Huse and E. C. Holland, *Nat. Rev. Cancer* 2010, **10**, 319.
2 a) Y. Chen, G. Dalwadi, H. A. E. Benson and V. Kakkar, *Cur. Durg Deliv.* 2004, **1**, 361; b) I. Rooy, S. C.Tascioglu, W. E. Hennink, G. Storm, R. M. Schiffelers and E. Mastrobattista, *Pharm. Res.* 2011, **28**, 456.
3 R. Daneman, *Ann. Neurol.* 2012, **72**, 648.
4 R. Cecchelli, V. Berezowski, S. Lundquist, M. Cilot, M. Renftel, M. P. Dehouck and L. Fenart, *Nat. Rev. Drug Discovery* 2007, **6**, 650.
5 a) R. M. Koffie, C. T. Farrar, L. J. Saidi, C. M. William and B. T. Hyman, *PNAS*. 2011, **108**, 18837; b) D. Ni, J. Zhang, W. Bu, H. Xing, F. Han, Q. Xiao, Z. Yao, F. Chen, Q. He, J. Liu, S. Zhang, W. Fan, L. Zhou, W. Peng and J. Shi, *ACS Nano* 2014, **8**, 1231.
6 R. Qiao, Q. Jia, S. Huwel, R. Xia, T. Liu, F. Gao, H. -J. Galla and M. Gao, *ACS Nano* 2012, **6**, 3304.
7 M. F. Warsi, R. W. Adams, S. B. Duckett and V.Chechik, *Chem. Commun.l* 2010, **46**, 451-453.
8 L. Li, M. Nurunnabi, Y. Y. Jeong, Y. Lee and K. M. Huh, *J. Mater. Chem. B* 2014, **2**, 2929.
9 C. H. Su and F. Y. Cheng, *RSC Advances* 2015, **5**, 90061.
10 T. Sun, Y. S. Zhang, B. Pang, D. C. Hyun, M. Yang and Y. Xia, *Angew. Chem. Int. Ed.* 2014, **53**, 12320.

11 W. Yuan, G. Li and B. M. Fu, *Ann. Biomed. Eng.* 2010, **38**, 1463.
12 a) J. V. Georgieva, R. P. Brinkhuis, K. Stojanov, C. A. G. M. Weijers, H. Zuilhof, F. P. J. T. Rutjes, D. Hoekstra, J. C. M. van Hest and I. S. Zuhorn, *Angew. Chem. Int. Ed.* 2012, **51**, 1; b) Y. Zhang, W. Zhang, A. H. Johnston, T. A. Newman, I. Pyykko, J. Zou, *Int. J. Nanomedicine* 2012, **7**, 1015.
13 H. Xin, X. Y. Jiang, J. J. Gu, X. Y. Sha, L. C. Chen, K. Law, Y. Z. Chen, X. Wang, Y. Jiang and X. Fang, *Biomaterials* 2011, **32**, 4292.